Chapter

Decoupled and Descattered Monopole MIMO Antenna Array with Orthogonal Radiation Patterns

Hussain Al-Rizzo, Ayman A. Isaac, Sulaiman Z. Tariq and Samer Yahya

Abstract

This chapter introduces a novel design concept to reduce mutual coupling among closely-spaced antenna elements of a MIMO array. This design concept significantly reduces the complexity of traditional/existing design approaches such as metamaterials, defected ground plane structures, soft electromagnetic surfaces, parasitic elements, matching and decoupling networks using a simple, yet a novel design alternative. The approach is based on a planar single decoupling element, consisting of a rectangular metallic ring resonator printed on one face of an ungrounded substrate. The decoupling structure surrounds a two-element vertical monopole antenna array fed by a coplanar waveguide structure. The design is shown both by simulations and measurements to reduce the mutual coupling by at least 20 dB, maintain the impedance bandwidth over which S_{11}, is less than −10 dB, and reduce the envelope correlation coefficient to below 0.001. The boresight of the far-field radiation patterns of the two vertical monopole wire antennas operating at 2.4 GHz and separated by 8 mm ($\lambda_o/16$), where λ_o is the free-space wavelength at 2.45 GHz, is shown to be orthogonal and inclined by 45° with respect to the horizontal (azimuthal) plane while maintaining the shape of the isolated single antenna element.

Keywords: 4G/5G LTE/LTE-A, cellular communications, coplanar waveguide fed vertical monopole, decoupled antenna array, descattered antenna array, GPS, microstrip fed vertical monopole, MIMO, radar, RFID, Wi-Fi, WiMAX

1. Introduction

Contemporary wireless systems including, but not limited to, 4G/5G LTE/LTE-A, radar, RFID, Wi-Fi, WiMAX, GPS, geolocation, biomedical imaging, and remote sensing dictate the use of miniaturized MIMO antenna arrays on mobile terminals. They can also be permanently installed on fixed structures for increased gain, which will improve link reliability and quality of service, increase communication range, and increase battery life through a variety of diversity schemes [1, 2], and/or increase data rate/throughput through MIMO spatial multiplexing schemes [3].

Moreover, these structures can provide esthetic, miniaturized wireless consumer devices. Recent trends toward miniaturized, esthetically appealing, battery efficient handheld wireless devices, and green wireless systems require antenna arrays that should be implemented within a restricted physical space.

In this chapter, we report a new approach of how to reduce the complexity of prior existing designs for mutual coupling reduction such as periodic metamaterial/metasurface constructs [4–8], defected ground plane structures [9, 10], soft/hard electromagnetic surfaces [11, 12], parasitic elements [13], matching and decoupling networks [14–16], and neutralization lines [17]. Our proposed approach can still maintain, and in certain circumstances exceed the performance metrics of traditional approaches well-known in previous art, [18–20] using much simpler, cost-effective, and novel design alternatives.

Numerous techniques were proposed for the mutual coupling reduction among the elements of MIMO antenna arrays, the most notable and highly embraced is the use of metamaterials, which subsequently turned into an unique topic of its own used in various disciplines including acoustics, RF, optics, laser, and nanotechnology [21]. A defected ground plane consisting of a slitted pattern is disclosed in [9] to suppress mutual coupling between two monopole antennas separated by 0.093 λ_0, where λ_0 is the free-space wavelength at 2.53 GHz. The two monopoles share a 40 × 25 mm ground plane and are separated by 11 mm. Each slit is 11 × 1 mm. A periodic array of three slits was used to achieve a mutual coupling better than −20 dB. However, no information on the behavior of far-field radiation patterns of the array was provided. A simple yet elegant decoupling approach was presented in [22] using a parasitic element to decouple two monopole antennas operating at 900 MHz. The parasitic element is situated at the center between the two driven elements on a 330 × 250 mm FR4 substrate, 1.5 mm in thickness. The substrate has a permittivity of 4.4 and a loss tangent of 0.02. The radiation behavior shows an end-fire pattern. The measured pattern correlation is close to 0.02. This method achieved coupling coefficient, S_{12} close to −40 dB over the bandwidth in which S_{11} is less than −10 dB. The method requires careful attention to the choice of the distance between the parasitic element and the driven elements for a given separation between the driven elements. A drawback of this technique is the undesired radiation from the parasitic element, which may degrade the decoupled radiation pattern.

A complicated approach for mutual coupling suppression between two monopole antennas operating at 2.49 GHz and separated by 0.09 λ_0, where λ_0 is the free-space wavelength at 2.49 GHz, with a length of 32.5 mm over a ground plane containing four slits, 1 × 11 mm in size and two defected wall structures situated at the edge of the outermost slits are proposed in [20]. The defected wall structure consists of a metallic plane with C-shaped cuts mimicking split ring resonators. The spacing between the slots in the defected wall is 0.09 λ_0. The structure achieved a measured isolation of about 44 dB. No information has been provided on the shape of the far-field radiation patterns. One notable approach for the isolation of two high-profile monopole antennas laid on a common copper ground plane (1.25 λ_0 × 1.25 λ_0), involves the use of highly negative-permeability, broadside coupled split-ring resonators etched on both sides of a dielectric substrate. In this approach, the two monopoles are separated by λ_0/8 (30.25 mm), where λ_0 is the free-space wavelength at 1.24 GHz [18]. A 3-D stack employing 10 arrays is aligned vertically using plastic support in the space between the two monopoles, where each array consists of four broadside coupled split-ring resonators.

It should be noted, however, that these artificial magnetic inclusions obviously suffer from extremely narrow resonance bandwidth. The design methodology is

based on creating artificial negative permeability, which consequently presents extremely high attenuation to the near-field that exists in the region between the two monopoles for both propagating and evanescent fields. The authors claim a reduction of at least 20 dB in S_{12} but over an extremely small bandwidth. The structure is neither convenient nor rigid for miniaturized handheld devices since the decoupling structure occupies a significant volume in the space between the two monopoles. Also, the fabrication costs as well as the dielectric and conductor losses introduced by the decoupling structure even at frequencies in the decoupled regime create an inconvenience. We should note that a similar approach was reported in [19] in which a metamaterial spacer is employed to reduce the mutual coupling between two monopoles, each 27.8 mm in height, installed on a common ($2\,\lambda_0 \times 2\,\lambda_0$) aluminum ground plane and separated by $0.156\,\lambda_0$ (18 mm) at 2.6 GHz. The principle of operation is explained by considering the metamaterial acting as an artificial magnetic conductor (AMC). The decoupling structure consists of four existing design of a bidirectional AMC printed on a dielectric substrate with width-height-thickness dimensions of 64 × 33 × 10.5 mm.

Several defected ground planes [9–12], soft artificial electromagnetic surfaces, matching and decoupling networks [14–16], and neutralization lines [17] have received considerable recent research interest in both academia and industry. However, they were not applied specifically to vertical monopole antennas, the subject of this chapter. It should be noted that these traditional approaches suffer from:

a. Extremely narrow bandwidths since metamaterials, defected ground structures, and soft electromagnetic surfaces embrace inherently high-resonant structures;

b. Repeated periodic structures are employed periodically in 1-D, 2-D, or in 3-D using vias, which further complicates the design and increases the fabrication cost;

c. Insertion of many 2D cells (arranged in multiple rows and/or columns) and sometimes 3D unit cells [7, 8] between the antenna elements limits the empty space between the antenna elements and hence complicates the task of miniaturizing the MIMO antenna array; and

d. Distortion of the far-field radiation patterns and/or reduction the operating bandwidth [18–20] from these artificial structures.

To conclude, most of the related research utilized meta-surfaces inclusions inserted in the space *between* the antenna elements for which the mutual coupling is to be reduced. This is another major obstacle for applications involving extremely miniaturized antenna arrays, such as MIMO systems on handheld wireless devices. In this chapter, however, we report a novel approach in which the mutual coupling is reduced by inserting two vertical monopole antenna elements *inside* a rectangular conducting ring loaded with two conducting strips. This technique allows much smaller separations ($\lambda_o/16$), where λ_o is the free-space wavelength. Unlike the traditional techniques that are based on inserting artificial resonant structures between the radiating elements, the methodology reported in this chapter is based on *enclosing* the radiating elements by simple and versatile planar conducting structures, the performance of which exceeds the performance of traditional/existing design approaches.

2. MIMO array structure

We will elaborate on one embodiment involving a miniaturized two-element antenna array system composed of two vertical monopole antennas separated by 8 mm, corresponding to $\lambda_o/16$, where λ_o is the wavelength in free space at 2.4 GHz. The unique design scheme of the coupled array produces orthogonal radiation patterns even without the inclusion between the monopoles. Additionally, the decoupling structure is designed to reduce the mutual coupling and enhance isolation between the signals at the array terminals. A very low envelope correlation coefficient between the received signals is realized to accommodate operating with the different MIMO modes. To summarize, the design of the antenna array disclosed in this chapter seeks to achieve three functions: decoupling, descattering, and orthogonalization of the far-field radiation patterns in the boresight directions. Descattering in this context implies that the radiation pattern of each antenna element in the array is the same as the radiation pattern when in isolation.

To obtain a boresight oriented by 45° relative to that of a conventional vertical monopole, the design uses a partial reference ground plane instead of a traditional full ground as shown in **Figure 1**. The monopole is mounted on a dielectric substrate and is fed by a coplanar waveguide (CPW) circuit. The ground plane of the coplanar feeding circuit serves as a partial ground for the antenna as well. The height of the monopole h and the feeding circuit geometry are tuned such that the antenna operates at center frequency of 2.4 GHz serving applications in the ISM band. The coplanar waveguide feeding circuit is selected to have a characteristic impedance of 50 ohm at its input. The geometry, reflection coefficient, and radiation pattern of the single element are shown in **Figures 1**–**3**, respectively.

This behavior is exploited to construct an array consisting of two vertical monopoles, the radiation patterns of which are identical in shape but orthogonally oriented in space. The antenna array is formed by placing monopole 2 and its feeding circuit as a mirror image of monopole 1 around the y-z plane as depicted in **Figure 4**. Both antennas are assembled on a common substrate of a relative permittivity, ε_r = 10.2, and height, h_s = 1.27 mm.

When the two antennas are positioned in a close proximity, $\lambda_o/16$, in this design, the far-field radiation patterns will be distorted while the correlation coefficient

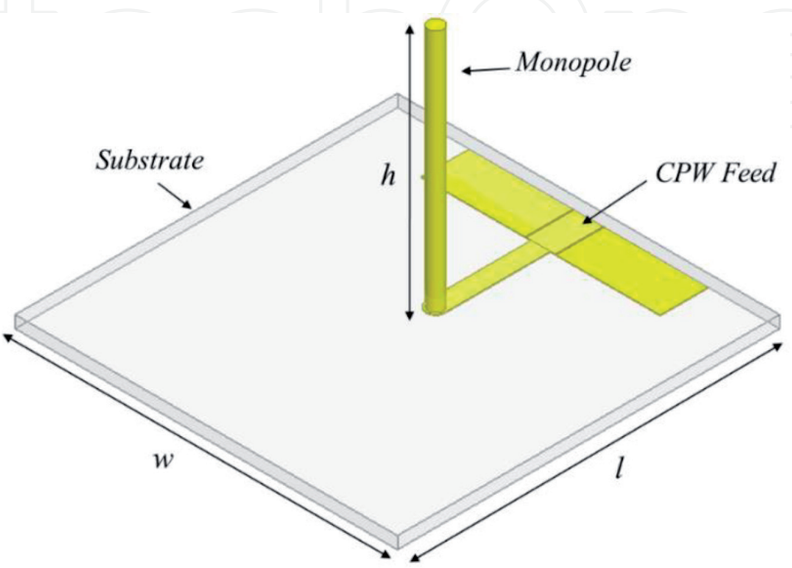

Figure 1.
Geometry of a single monopole antenna fed by CPW.

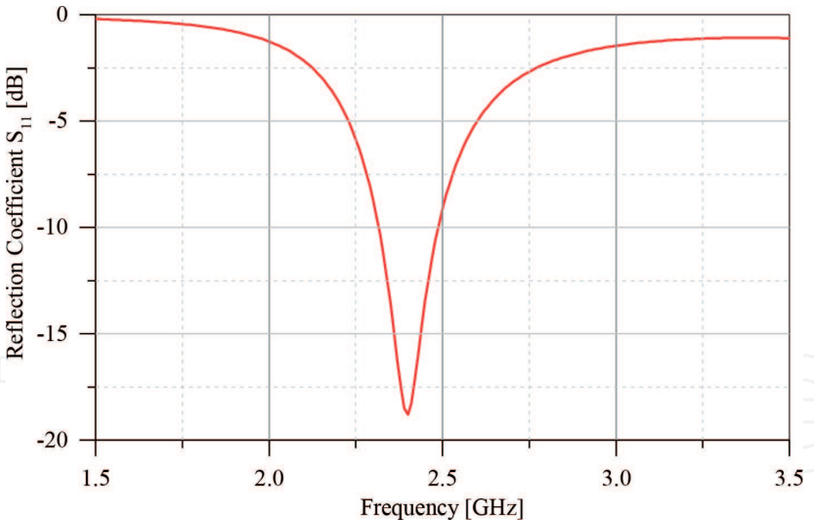

Figure 2.
Reflection coefficient of the monopole antenna fed by a CPW.

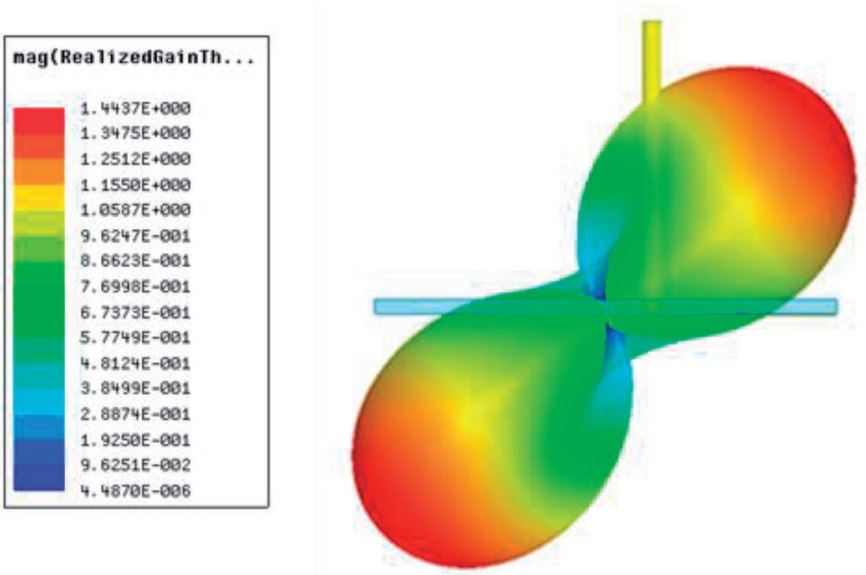

Figure 3.
Realized gain of the monopole antenna fed by a CPW.

increases due to mutual coupling. To investigate the mutual coupling effects, the array is simulated using the commercial software package, high-frequency structure simulator (HFSS) of ANSYS. The geometry of the design is shown in **Figure 5** and the dimensions are presented in **Table 1**.

Despite the reduction in transmission level between the feeding ports, the distribution of surface currents depicted in **Figure 6**, resulted from exciting port 1 while terminating port 2 with 50 ohms, shows the existence of significant interfering currents distributed on the CPW feeding of monopole 2. The current induced on monopole 2 and its feeding circuitry is due to the mutual coupling between the two antennas.

In **Figure 7**, we show the reflection coefficient, S_{11} and transmission coefficient, S_{21} plotted against frequency. The coupled array provides a bandwidth of 230 MHz over which the reflection coefficient is below −10 dB. At 2.4 GHz, the partial ground plane reduced S_{21} to −10 dB compared to −4 dB if the antennas share a common full ground plane and are separated by 8 mm. The radiation patterns in terms of the realized gain are plotted in **Figure 8** for two cases; in the first case, an

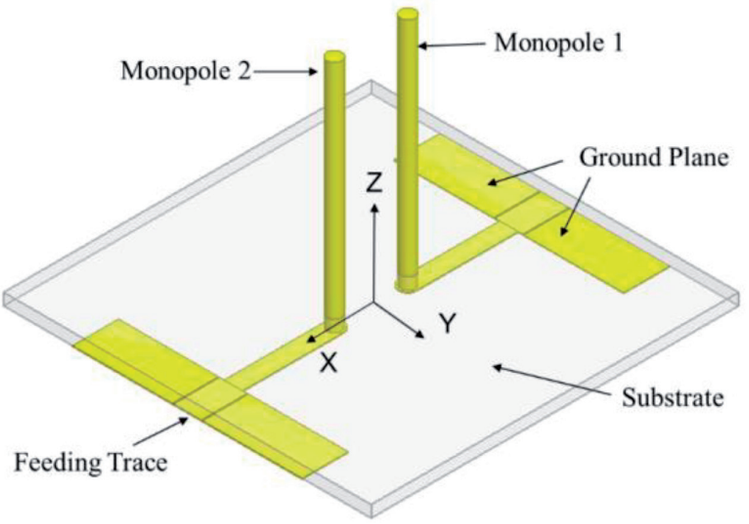

Figure 4.
The coupled monopole antenna array.

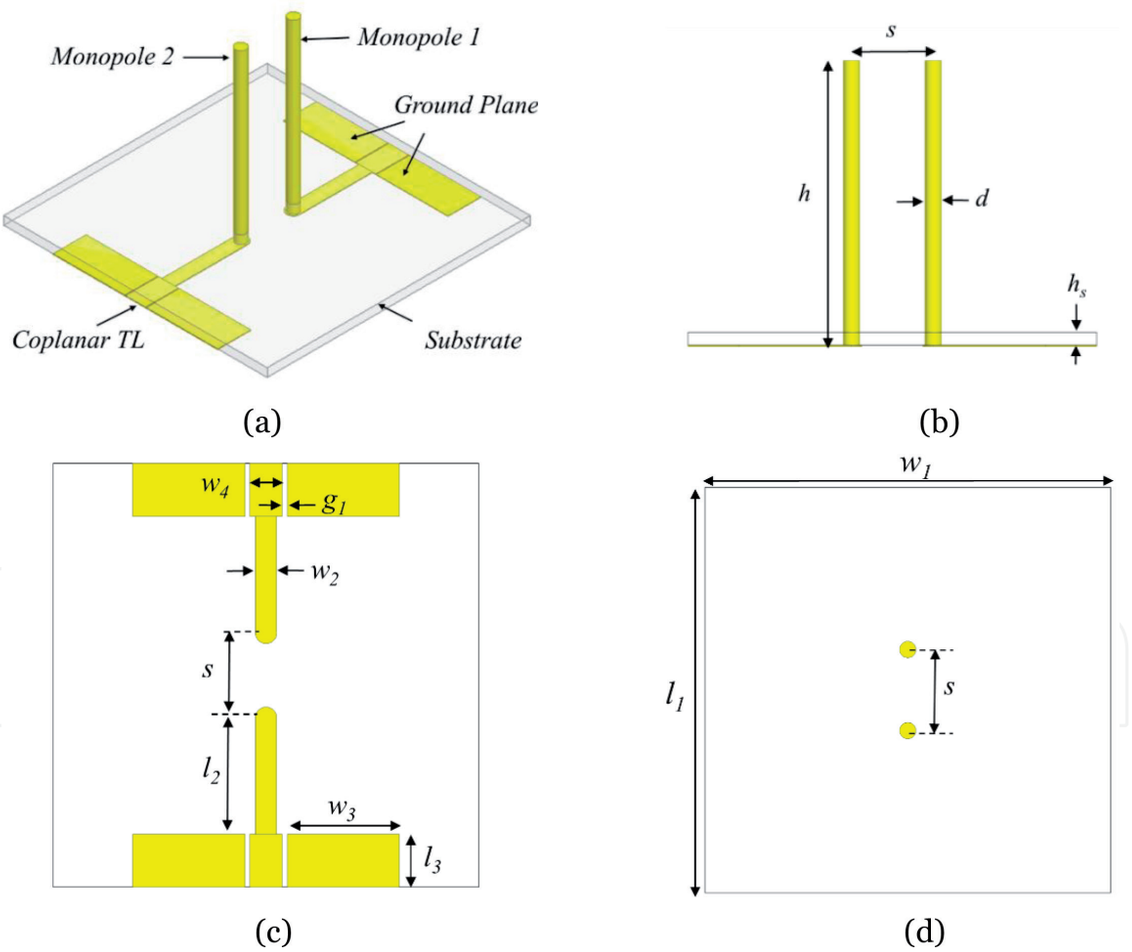

Figure 5.
Geometry of the coupled antenna array. (a) Prospective view, (b) Side view, (c) Bottom view and, (d) Top view.

excitation signal is injected into port 1, while the second port is terminated with its internal impedance, 50 ohms. In the second case, the excitation signal is injected into port 2, and port 1 is terminated by 50 ohms. Having the antennas placed extremely close to each other (8 mm at 2.4 GHz) resulted in disturbing the near

Monopoles separation (s)	8
Monopole height (h)	25
Monopole diameter (d)	1.6
Feeding probe length(l_2)	11
Feeding probe width (w_2)	2
Ground width (w_3)	10.85
Ground length (l_3)	5
Center strip width (w_4)	3
CPW gap width (g_1)	0.5
Substrate ($l_1 \times w_1 \times h_s$)	(40 × 40 × 1.27)
Dielectric constant (ε_r) of the substrate	10.2

Table 1.
Dimensions of the coupled antenna Array.

field and increasing the coupling level. This proximity causes the radiation patterns to be directed into the lower part below the plane containing the substrate.

The proposed MIMO antenna array consists of two monopole antennas positioned on a printed circuit board. The antennas are surrounded by a decoupling circuit printed on the top side of the substrate and a feeding circuit on the bottom side. For short, the design will be called the decoupled coplanar waveguide fed monopole antenna array (CPW-MAA). The substrate has a length and width of 40 × 40 mm, and a thickness of 1.27 mm.

In order to further enhance the performance of pattern diversity for the two-element antenna array and minimize the contribution of mutual coupling among the elements of the antenna array to the channel correlation, the mutual coupling effect needs to be reduced with minimal distortion to the radiation patterns of the individual elements, preferably such that the 3-D far-field patterns of the individual elements being identical in shape and orthogonal in space. This applies to the signals at the output of the antennas when transmitting and at the input of the feeding circuit when operating in the receive mode.

The decoupling structure, shown in **Figure 9**, consists of a simple 2D planar rectangular metallic ring and two tuning metallic strips printed on the surface of the substrate.

First, the performance of the CPW-MAA is compared against the coupled monopole antenna array shown in **Figure 5** using the same substrate. Furthermore, as a design alternative and to further validate the disclosed design concept, another substrate has been used with a dielectric constant ε_r of 6.15 and height, 1.27 mm. Each monopole is fed by a copper trace printed on the bottom side of the substrate. Each monopole makes a contact with the copper trace by extending the monopole body inside the substrate to reach the feeding copper trace at the bottom layer. A CPW at the bottom side of the substrate is used to deliver the signal to the antennas in case of transmitting and from the antennas in case of receiving.

The CPW consists of a central strip having a length of l_3 and a width of w_4 with the finite ground planes positioned on both sides of the central strip with a width of w_3. An SMA is utilized to launch the wave into the array. The impedance of the SMA is 50 ohm and is used to connect the antenna to a vector network analyzer used in the measurements. The array system dimensions are tuned to operate at a

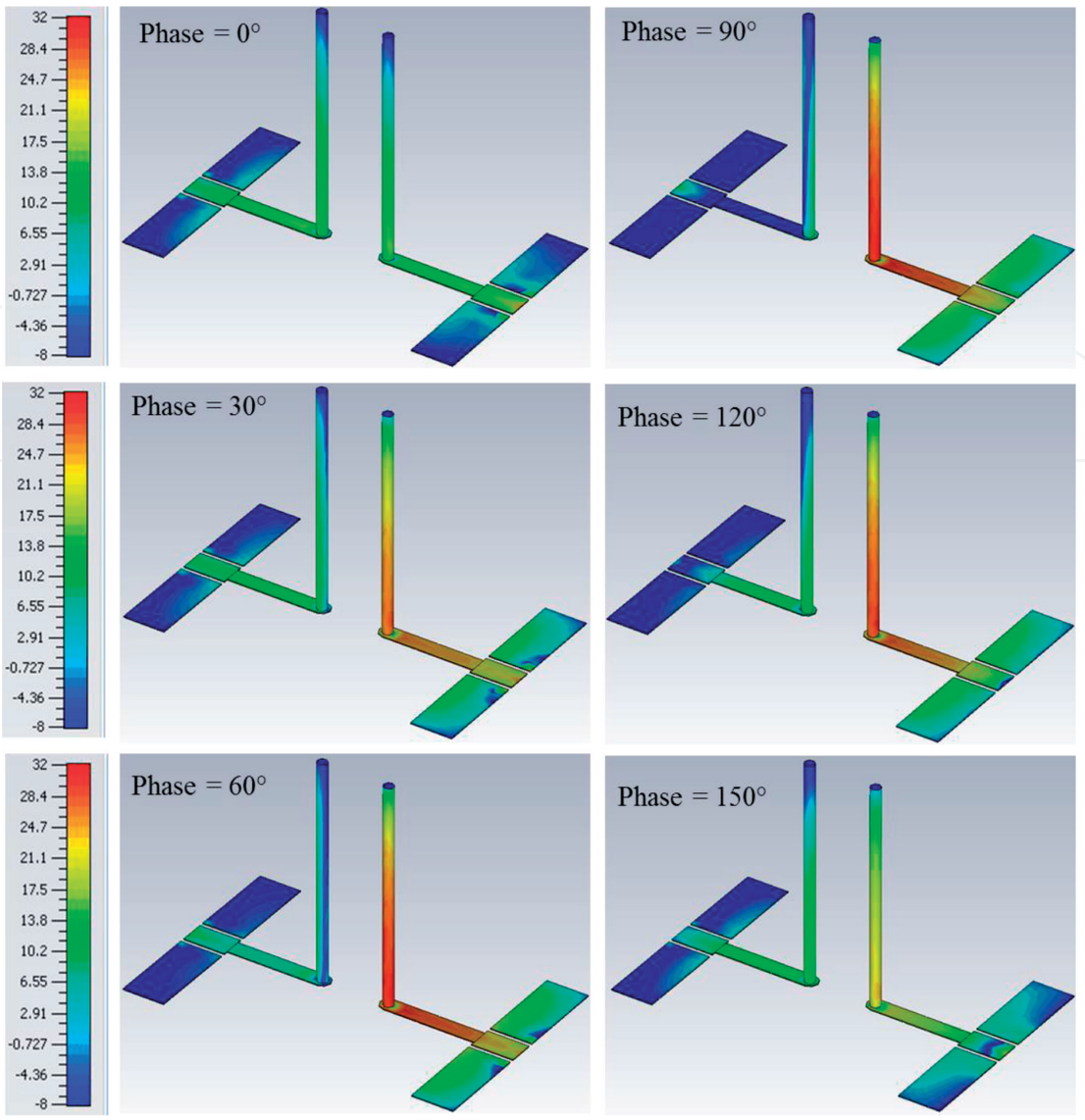

Figure 6.
Magnitude of surface current distribution for the coupled monopole antenna array, dB(1 A/m).

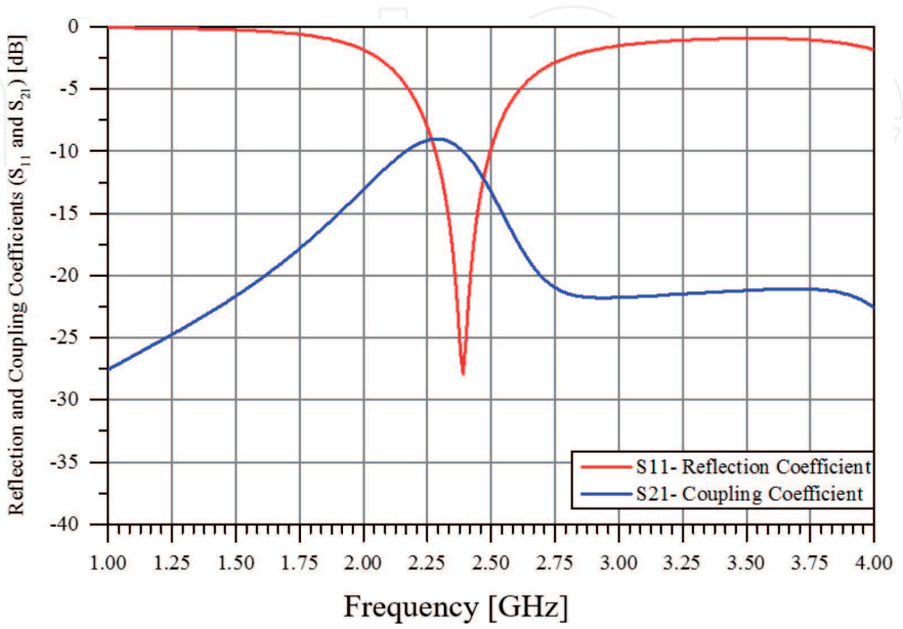

Figure 7.
Frequency response of the coupled monopole antenna.

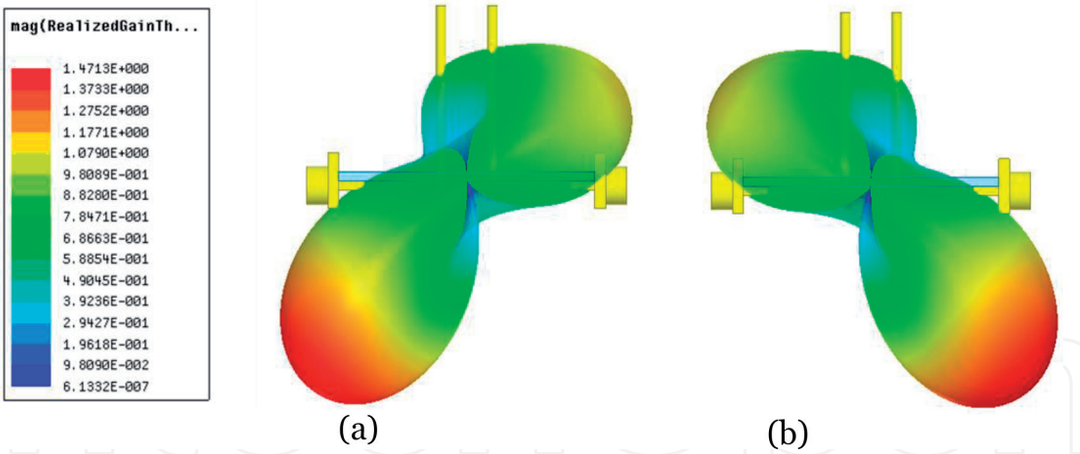

Figure 8.
Mutual coupling effects on the far-field radiation patterns. (a) Exciting port 1 and, (b) Exciting port 2.

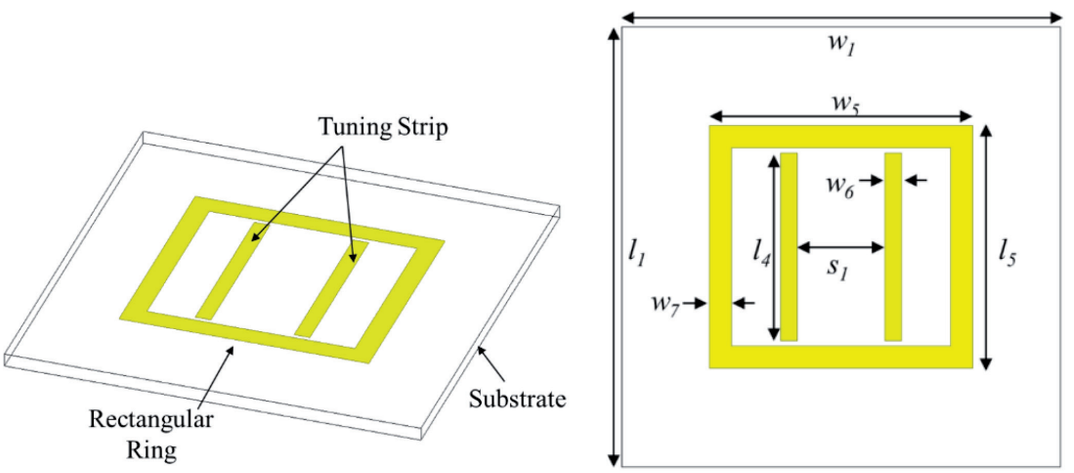

Figure 9.
Decoupling circuit.

2.4 GHz with a bandwidth of 260 MHz over which the reflection coefficients, S_{11} and S_{22}, are less than −10 dB and transmission coefficients, S_{12} and S_{21} less than −20 dB. The two-element MIMO antenna array is shown in **Figure 10**, while dimensions are depicted in **Table 2** for the two substrates used where all dimensions are in millimeters.

Prototypes are fabricated and measured at the University of Arkansas at Little Rock's Antennas and Wireless Systems Research Laboratory (AWSRL). The prototype which is shown in **Figure 11** used Roger RO3210 substrate. The frequency response has been measured using E5071B and N5242A VNAs. The radiation patterns are measured inside an anechoic chamber. Using Roger RO3210 (dielectric constant ε_r of 10.2) as a substrate, and in order to demonstrate that adding this decoupling circuit isolates the input and output ports, the magnitude of the surface current dB (1 A/m) has been plotted for different excitation phase delays as depicted in **Figure 12**. A signal of 1 W is assigned through port 1 to excite the first monopole, the monopole in the right side of the array, while port 2 is terminated by its internal impedance of 50 ohm. It seems quite evident that the amount of current coupled to the feeding circuit of monopole 2 at different phase delays is very low, minimum at −8 dB (1 A/m) (blue color), compared to other excited monopole, where a high current is observed with a maximum value at 32 dB (1 A/m) (red color). This contrast of 40 dB (1 A/m) reveals the high isolation level achieves due

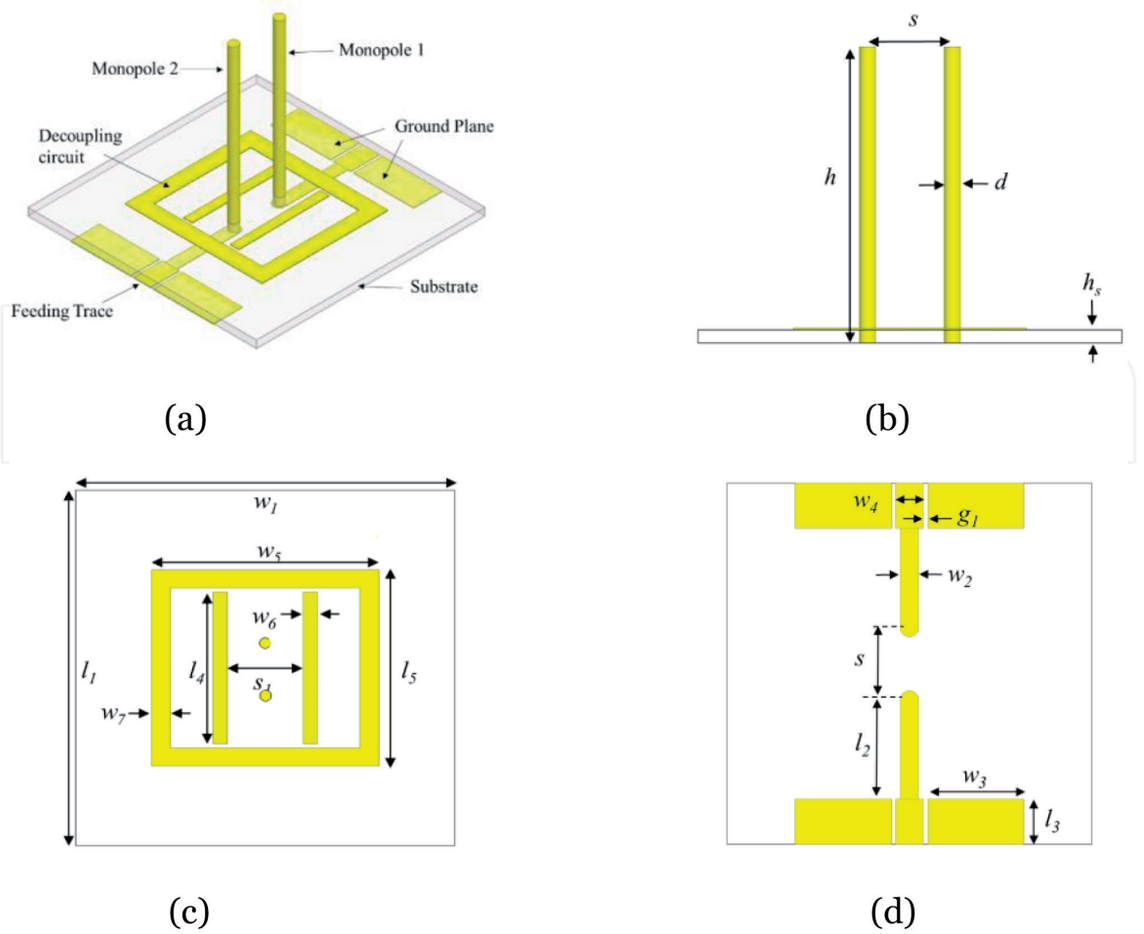

Figure 10.
The decoupled CPW-MAA. (a) Prospective view, (b) Side view, (c) Top view, (d) Bottom view.

Dimension defined name	Substrate RO3210 ($\varepsilon_r = 10.2$)	Substrate RO3006 ($\varepsilon_r = 6.15$)
Monopoles separation (s)	8	8
Monopole height (h)	28	27
Monopole diameter (d)	1.6	1.6
Feeding probe length (l_2)	11	11
Feeding probe width (w_2)	2	2
Ground width (w_3)	10.5	10.8
Ground length (l_3)	5.0	5.0
CPW trace width (w_4)	3.0	3.0
CPW gap width (g_1)	0.5	0.2
Rectangular ring outer length (l_5)	22	22
Rectangular ring outer width (w_5)	24	30
Rectangular ring trace width (w_7)	2.5	2.5
Tuning strip length (l_4)	16	16
Tuning strip width (w_6)	1.5	4
Tuning strips separation (s_1)	6.5	8
Substrate ($l_1 \times w_1 \times h_s$)	(40 × 40 × 1.27)	(40 × 40 × 1.27)

Table 2.
Dimensions of the CPW-MAA for two substrates.

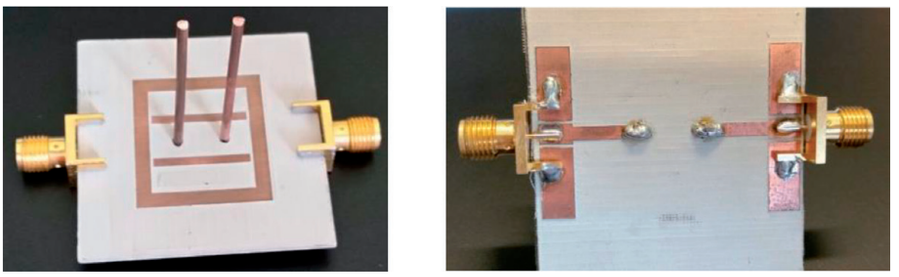

Figure 11.
The decoupled CPW-MAA and decoupled MS-MAA prototypes.

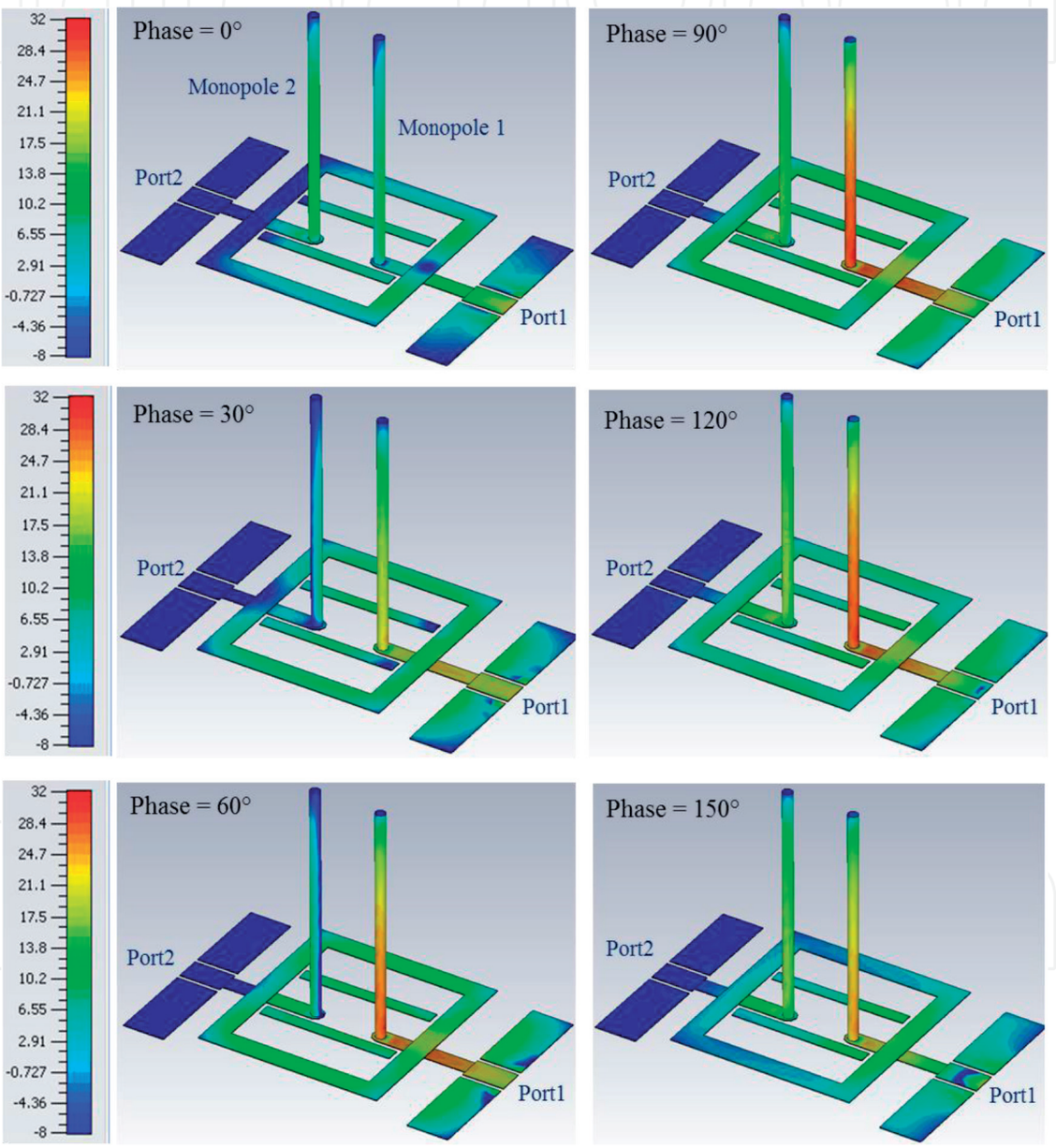

Figure 12.
Two monopole antenna array with decoupling network; surface current distribution (magnitude) dB(1 A/m).

to the decoupling network compared to the coupled current before adding the decoupling network shown in **Figure 6**.

The simulated and measured results of the scattering parameter, S_{11} are presented in **Figure 13**. The amount of coupling expressed in terms of scattering parameter, S_{21} is depicted in **Figure 14**. These figures reveal good agreement

between the simulated models and the measurements using the fabricated prototype.

Introducing the decoupling network resulted in a reduction of −19 dB in mutual coupling level, from −4 to −23 dB. The antenna array system offers a bandwidth of 10%, in which the coupling coefficient, S_{21} is less than −20 dB and 14% over which the reflection coefficient, S_{11} is less than −10 dB. The slight shift of 2% in the frequency at which the measured coupling coefficient S_{21} is at its minimum in the bandwidth of interest compared to simulated results is due to the variations associated with the fabrication of the prototype and the limited precision of simulations and measurements. The fabricated prototype also provides a wider bandwidth. This is due to the dielectric and metallic losses inherent in the substrate and dipoles, which lead to reduced Q factor.

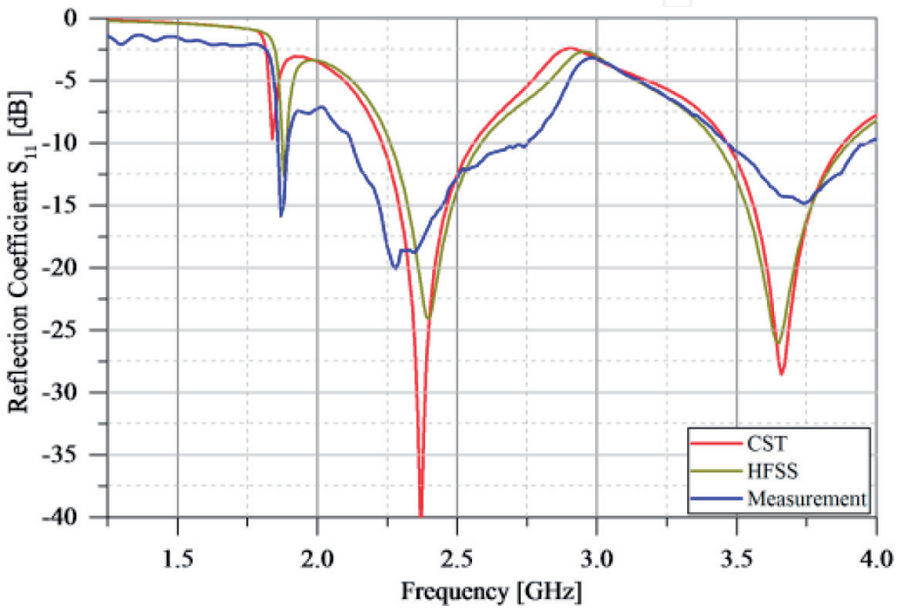

Figure 13.
Reflection coefficient S_{11}, simulation versus measurements.

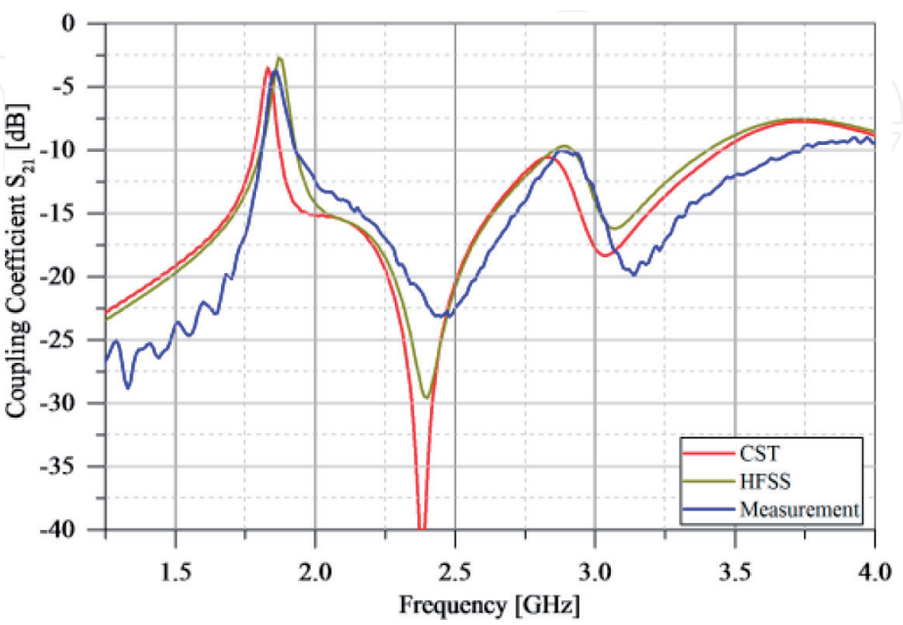

Figure 14.
Coupling coefficients S_{21}, simulation versus measurements.

Table 3 summarizes the performance metrics of the simulated models and the measured prototype. In this table, f_L and f_H denote the lower and upper frequency limits of the operating bandwidth, respectively. The array meets and exceeds the bandwidth requirement of 802.11 Wi-Fi systems operating in the ISM band at 2.4 GHz.

The maximum value of the total realized gain is plotted versus frequency in **Figure 15**. Another advantage of the proposed antenna array is the enhancement achieved in the realized gain and hence the efficiency. The total realized gain of a single element varies over the range from 1.6 to 1.69 dB over the frequency range 2.25–2.52 GHz over which S_{11} and S_{21} are less than −10 and −20 dB, respectively. This gain is obtained when one port is excited while the other is terminated with its characteristic impedance. An improvement of 2.1 dB is observed in the realized gain with the proposed antenna array as compared to a conventional array antenna consisting of two monopoles separated by $\lambda_0/16$ over a $\lambda_0 \times \lambda_0$ full ground plane. It is

Performance metric	Conventional array	HFSS	CST	Measured
S_{11} (min) dB	−8	−24	−40	−20
S_{22} (min) dB	−8	−23	−40	−33
S_{21} (min) dB	−4	−29	−45	−23
f_L (S_{11}, S_{22} < −10 dB) GHz	—	2.25	2.22	2.12
f_H (S_{11}, S_{22} < −10 dB) GHz	—	2.58	2.56	2.74
f_L (S_{12}, S_{21} < −20 dB) GHz	—	2.28	2.26	2.32
f_H (S_{12}, S_{21} < −20 dB) GHz	—	2.51	2.51	2.58
BW (S_{11}, S_{22} < −10 dB) GHz	—	0.33	0.34	0.62
BW (S_{21}, S_{12} < −20 dB) GHz	—	0.23	0.25	0.26
% BW (S_{11}, S_{22} < −10 dB)	—	13.6%	14.2%	25.5%
% BW (S_{21}, S_{12} < −20 dB)	—	9.6%	10.4%	10.6%

Table 3.
Decoupled array performance at 2.4 GHz in terms of scattering parameters (dB).

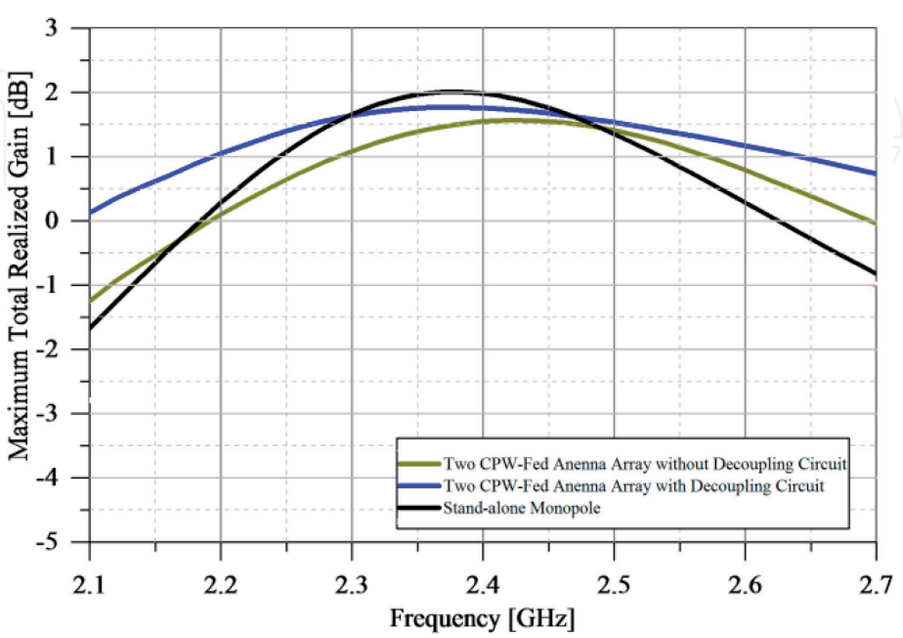

Figure 15.
Maximum realized gain.

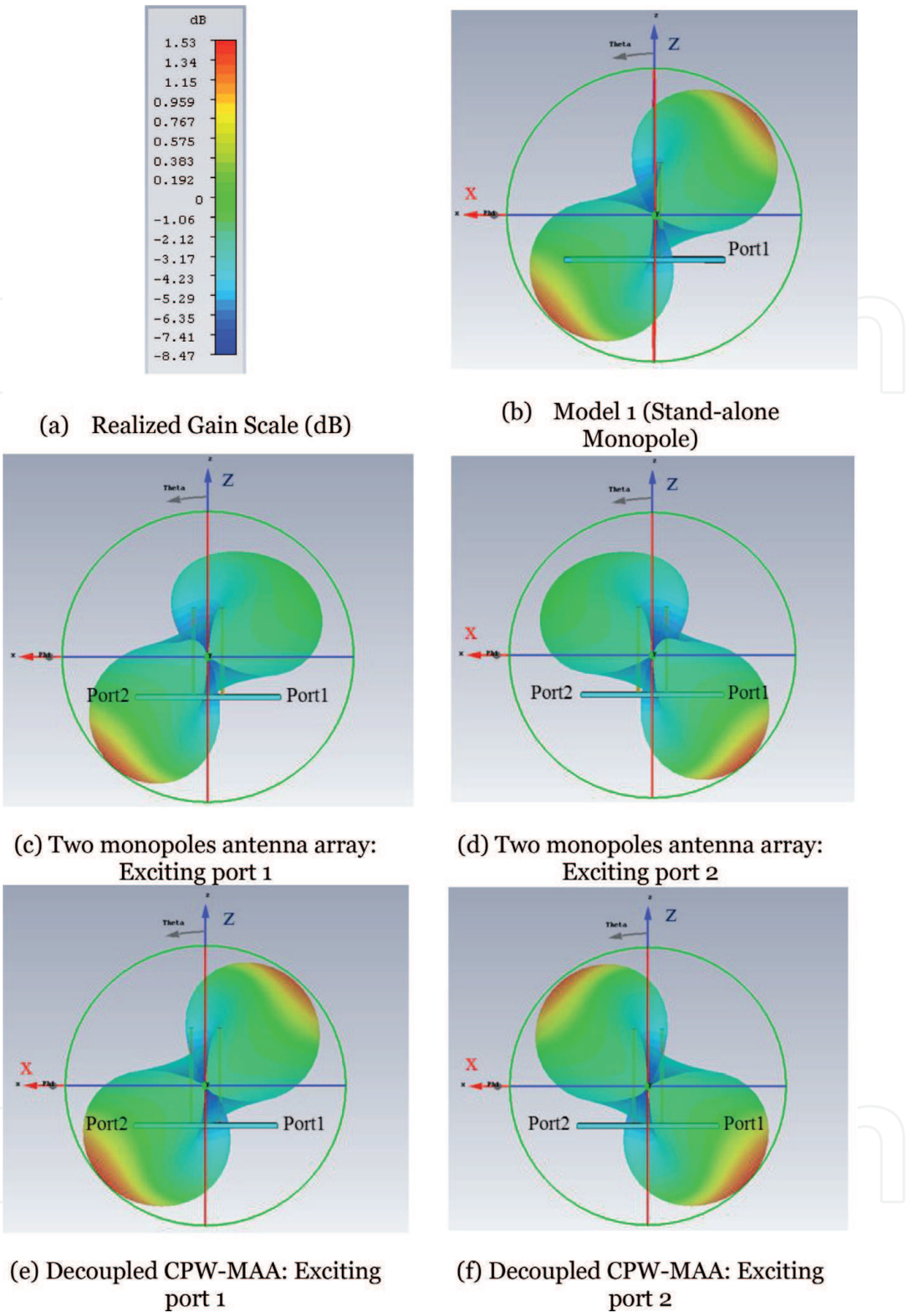

(a) Realized Gain Scale (dB)

(b) Model 1 (Stand-alone Monopole)

(c) Two monopoles antenna array: Exciting port 1

(d) Two monopoles antenna array: Exciting port 2

(e) Decoupled CPW-MAA: Exciting port 1

(f) Decoupled CPW-MAA: Exciting port 2

Figure 16.
(a) The realized gain scale. (b) Realized gain for a stand-alone monopole, while (c) and (d) are for the coupled monopole antenna array, then (e) and (f) are for the decoupled CPW-MAA. Examining the upper right section of the 3-D pattern of model 2, ($\pi \leq \phi \leq 2\pi$, and $\theta \leq \pi/2$) shows red spot, which indicates high gain which is reduced for the decoupled CPW-MAA, where more power is directed in the lower left side ($0 \leq \phi \leq \pi$ and $\theta \geq \pi/2$). This distortion has been corrected in the disclosed antenna array due to the low mutual coupling caused by adding the decoupling network. Furthermore, a descattered pattern is realized. **Figure 17** *shows a comparison between simulated and measured co/cross radiation patterns of the decoupled CPW-MAA (***Figure 18***).*

noteworthy that the maximum value of the total realized gain of the array system is close to that of a stand-alone monopole antenna.

The 3-D radiation patterns in terms of the realized gain are shown in **Figure 16**.

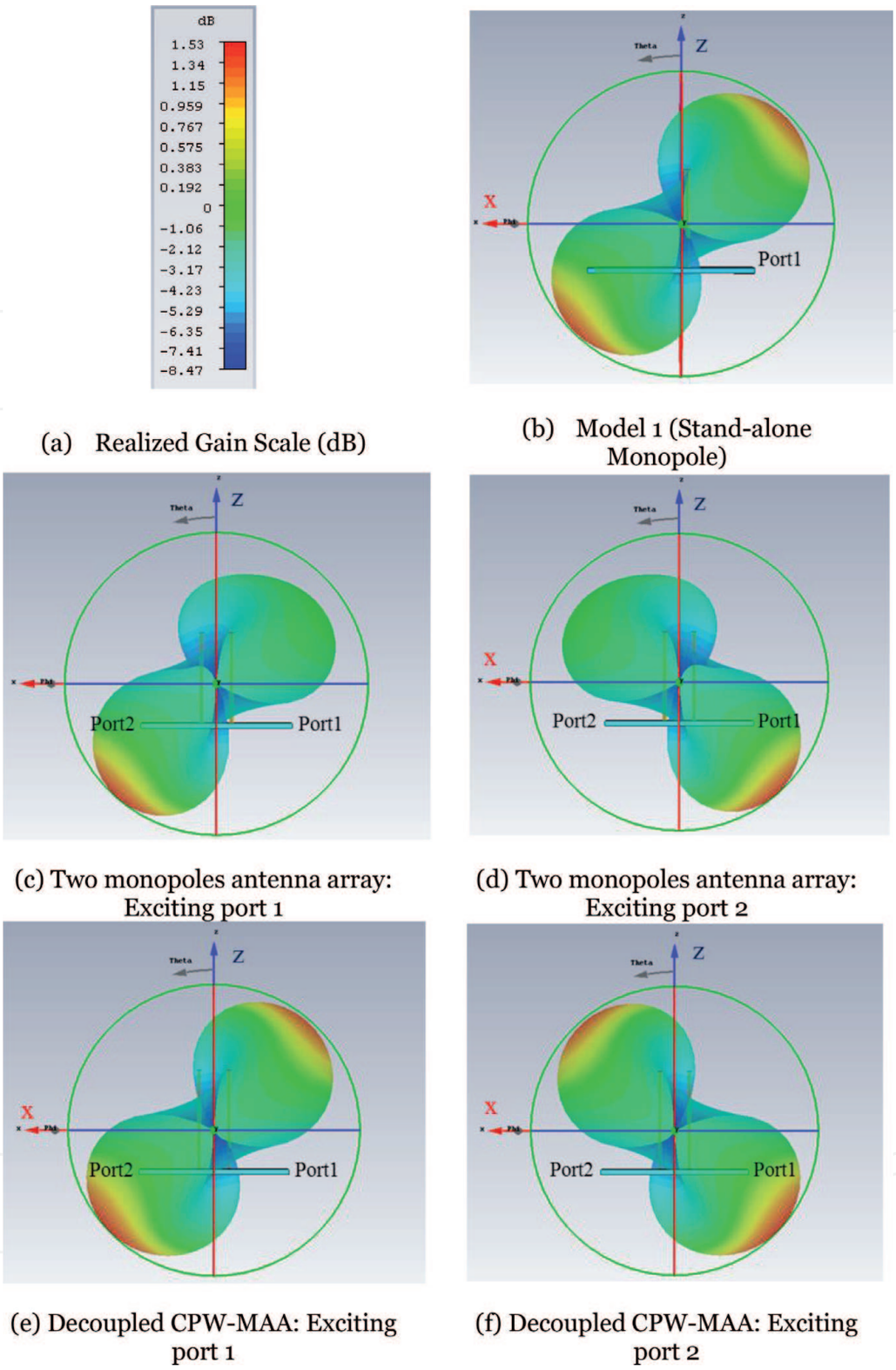

(a) Realized Gain Scale (dB)

(b) Model 1 (Stand-alone Monopole)

(c) Two monopoles antenna array: Exciting port 1

(d) Two monopoles antenna array: Exciting port 2

(e) Decoupled CPW-MAA: Exciting port 1

(f) Decoupled CPW-MAA: Exciting port 2

Figure 17.
Realized gain; scale (a), stand-alone monopole (b), two-monopole array without decoupling structure (c) and (d), decoupled CPW-MAA (e) and (f).

3. Conclusions

A compact MIMO antenna array with identical yet orthogonal radiation patterns and high isolation level is reported in this chapter. The shape and size of the partial ground plane and its distance from the monopole allowed the boresight of the radiation pattern of the isolated monopole to be oriented at an elevation angle

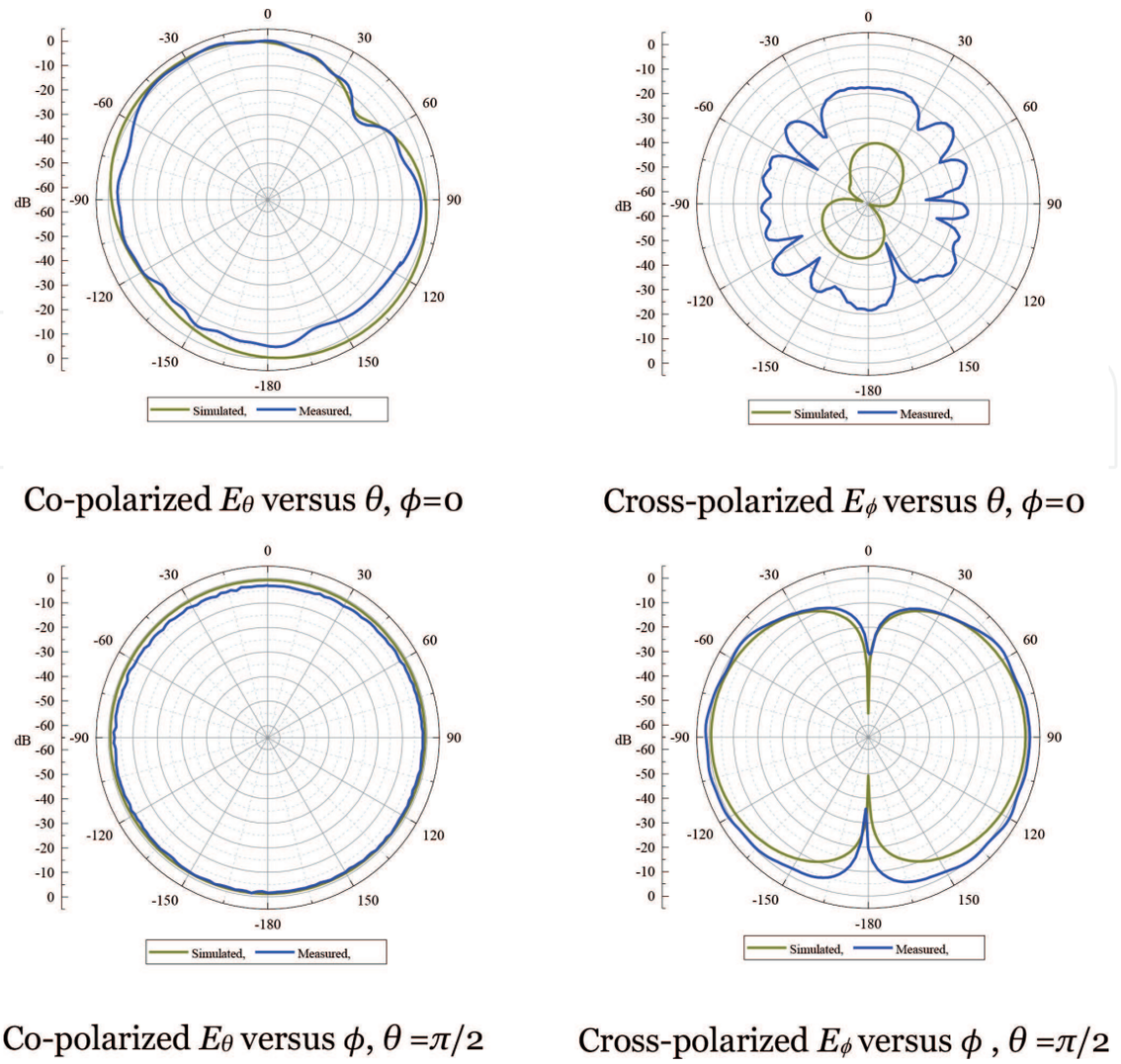

Figure 18.
Realized gain; simulation versus measurements.

of 45°. The 45° elevation achieved for the single monopole made it possible to place two vertical monopoles back to back to achieve an array with orthogonal radiation patterns. However, the mutual coupling between the two elements when placed in close proximity resulted in a distortion of the radiation patterns. To mitigate the effects of mutual coupling and increase the isolation between the two ports of the array, a decoupling element that surrounds the array elements which provides more flexibility on how close the elements need to be from each other. The dimensions of the rectangular ring and the tuning strips have been tuned to achieve the desired isolation level and restore the radiation pattern of the isolated element. The CPW-MAA with orthogonal far-field radiation patterns opens new opportunities for modern handheld devices and/or fixed wireless access points implementing MIMO techniques. Unlike existing design approaches that are based on inserting artificial resonant structures between the radiating elements, the design presented in this chapter encloses the radiating elements by simple and versatile planar conducting structures. The proposed design is demonstrated by simulations and measurements to significantly reduce the mutual coupling when the monopoles are spaced by 8 mm (λ_o/15.3). The performance achieved in terms of impedance matching, isolation, gain, bandwidth, and radiation pattern is comparable to network decoupling and parasitic approaches and better in terms of bandwidth, size, and complexity in comparison to existing designs which employ periodic AMC. A matching

bandwidth of 0.634 GHz over which the reflection coefficient, S_{11} is less than −10 dB, and a 0.246 GHz bandwidth over which the transmission coefficient, S_{21} is less than −20 dB have been achieved. A total realized gain of 1.69, 1.95, and 1.68 dB are achieved at 2.26, 2.4, and 2.52 GHz, respectively.

Author details

Hussain Al-Rizzo*, Ayman A. Isaac, Sulaiman Z. Tariq and Samer Yahya
Department of Systems Engineering, George W. Donaghey College of Engineering and Information Technology, University of Arkansas at Little Rock, Little Rock, AR, USA

*Address all correspondence to: hmalrizzo@ualr.edu

References

[1] Clerckx B, Oestges C. MIMO Wireless Networks Channels, Techniques and Standards for Multi-Antenna, Multi-User and Multi-Cell Systems. 2nd ed. Amsterdam: Academic Press; 2017

[2] MMda S, Monteiro FA. MIMO Processing for 4G and beyond: Fundamentals and Evolution. Boca Raton: CRC Press; 2016

[3] Hampton JR. Introduction to MIMO Communications. Cambridge: Cambridge University Press; 2014

[4] Sievenpiper D, Zhang L, Broas R, Alexopolous N, Yablonovitch E. High-impedance electromagnetic surfaces with a forbidden frequency band. IEEE Transactions on Microwave Theory and Techniques. 1999;**47**(11):2059-2074

[5] Yablonovitch E. Circuit and Method for Eliminating Surface Currents on Metals. 2001

[6] Kawaguchi K, Sugimoto Y, Kondo A, Yukumatsu M. Antenna Apparatus Having Patch Antenna. 2016

[7] Dandekar K, Mookiah P. MIMO Antenna Arrays Built on Metamaterial Substrates. 2016

[8] Mookiah P, Dandekar K. Bi-Directional Magnetic Permeability Enhanced Metamaterial (MPEM) Substrate for Antenna Miniaturization. 2015

[9] Murch R, Chiu C-Y, Rowell C. Systems and Methods Using Ground Plane Filters for Device Isolation. 2009

[10] Wu T-L, Hsu Y-H, Tsai C-H. Defected Ground Structure with Shielding Effect. 2010

[11] Abushamleh S, Al-Rizzo H, Kishk A, Abbosh A, Khaleel H. Miniaturized thin soft surface structure using metallic strips with ledge edges. Progress In Electromagnetics Research. 2014;**57**:221-232

[12] Abushamleh S, Al-Rizzo H, Abbosh A, Kishk A. Mutual coupling reduction between two patch antennas using a new miniaturized soft surface structure. In: 2013 IEEE International Symposium on Antennas and Propagation and USNC-URSI National Radio Science Meeting. 2013

[13] Kim C, Kim J, Choi C-G, Beak G, Park Y, Ahn H, et al. MIMO Antenna Having Parasitic Elements. 2013

[14] Zhao L, Wu K-L. A dual-band coupled resonator decoupling network for two coupled antennas. IEEE Transactions on Antennas and Propagation. 2015;**63**(7):2843-2850

[15] Zhao L, Yeung LK, Wu K-L. A coupled resonator decoupling network for two-element compact antenna arrays in Mobile terminals. IEEE Transactions on Antennas and Propagation. 2014;**62**(5):2767-2776

[16] Zhao L, Qian K-W, Wu K-L. A cascaded coupled resonator decoupling network for mitigating interference between two radios in adjacent frequency bands. IEEE Transactions on Microwave Theory and Techniques. 2014;**62**(11):2680-2688

[17] Håkansson M, Ying Z. Multiple-Input Multiple-Output (MIMO) Multi-Band Antennas with a Conductive Neutralization Line for Signal Decoupling. 2014

[18] Bait-Suwailam MM, Boybay MS, Ramahi OM. Electromagnetic coupling reduction in high-profile monopole antennas using single-negative magnetic Metamaterials for MIMO applications. IEEE Transactions on Antennas and Propagation. 2010;**58**(9):2894-2902

[19] Ferrer PJ, González-Arbesú JM, Romeu J. Decorrelation of two closely spaced antennas with a metamaterial AMC surface. Microwave and Optical Technology Letters. 2008;**50**(5):1414-1417

[20] Dadashzadeh G, Dadgarpour A, Jolani F, Virdee B. Mutual coupling suppression in closely spaced antennas. IET Microwaves, Antennas and Propagation. 2011;**5**(1):113

[21] Capolino F. Metamaterials Handbook. Boca Raton: CRC Press; 2009

[22] Lau BK, Andersen JB. Simple and efficient decoupling of compact arrays with parasitic Scatterers. IEEE Transactions on Antennas and Propagation. 2012;**60**(2):464-472